J. Fluid Mech. (2001), *vol.* 437, *pp.* 13–28. Printed in the United Kingdom

Wave focusing and ensuing mean flow due to symmetry breaking in rotating fluids

By LEO R. M. MAAS

Netherlands Institute for Sea Research, PO Box 59, 1790 AB Texel, The Netherlands

(Received 23 March 2000 and in revised form 7 December 2000)

Rotating fluids support waves. These inertial waves propagate obliquely through the fluid, with an angle that is fixed with respect to the rotation axis. Upon reflection, their wavelength is unchanged only when the wall obeys the local reflectional symmetry, that is, when it is either parallel or perpendicular to the rotation axis. For internal gravity waves in a density-stratified fluid, sloping boundaries thus break the symmetry of ray paths, in a two-dimensional container, predicting their focusing upon attractors: particular paths onto which the wave rays, and hence the energy, converge, and to which the wave energy returns after a small number of refections. Laboratory observations, presented here, show that, despite the intrinsic three-dimensionality of inertial waves, attractors still occur. The intensified wave energy on the attractor encourages centrifugal instabilities, leading to a mean flow. Evidence of this comes from dye spreading, observed to develop most rapidly over the location where the attractor reflects from the sloping wall, being the place where focusing and instabilities occur. This mean flow, resulting from the mixing of angular momentum, accompanying the intensification of the wave field at that location, has geophysical implications, because the ocean, atmosphere and Earth's liquid outer core can be regarded as asymmetrically contained. The relevance of wave focusing in a rotating, spherical shell, the modifications due to the addition of radial stratification, and its implications for observed equatorial current patterns and inertial oscillations are discussed. The well-known universality of oceanic, gravito-inertial wave spectra might reflect complementary, divergent (chaotic) wave-ray behaviour, which occurs in containers obeying the reflectional symmetry, but in which symmetry is broken in the horizontal plane. Periodic orbits still exist, but now repell.

1. Introduction

Like gravity in a density-stratified fluid, rotation provides 'elasticity' to a fluid (Kelvin 1880; Bjerknes *et al.* 1933), and Coriolis forces are restoring as long as the fluid's angular momentum increases with increasing radius (Rayleigh 1916). Despite the absence of density stratification, a homogeneous fluid can thus still be considered stably stratified, but now in terms of angular momentum and in a radial direction (Veronis 1970). While individually displaced particles move circularly in a plane normal to the rotation axis, displacements of patches of fluid involve pressure forces that drive motion in the axial direction too. With Ω denoting the angular frequency of the rotating fluid, perturbations of frequency $\sigma < 2\Omega$, known as (elastoid) inertial waves (Bjerknes *et al.* 1933), will therefore propagate obliquely through the rotating fluid (Görtler 1944), like internal gravity waves in density-stratified fluids (Görtler 1943). Their behaviour and fate is relevant to all rotating fluids occurring in nature

or industry, particularly, as shown in the experiment here, when through mixing they affect the wave's medium. Examples include stars (Gough & McIntyre 1998), planetary atmospheres (Bjerknes *et al.* 1933; Ushimara & Tanaka 1990), planetary cores (Aldridge & Lumb 1987; Olson & Aurnou 1999), oceans and lakes (LeBlond & Mysak 1978) and fluid-filled spinning spacecraft (Manasseh 1992).

The oblique propagation of inertial waves follows from the dispersion relation that monochromatic perturbations have to satisfy: $\sigma/2\Omega = \pm\sin\theta$, which shows that for fixed frequency, the direction in which energy propagates with respect to the rotation axis θ is fixed. This dispersion relation determines that phase and energy propagate in perpendicular directions, such that their horizontal components are in opposition. Observations of inertial waves invariably show this oblique and transverse propagation (Oser 1958; Fultz 1959) in closed cylindrical containers, often eventually displaying the so-called 'resonant collapse' – a violent, global 'breaking' of the oblique pattern of waves (McEwan 1970; Manasseh 1996).

The dispersion relation is obtained by substituting a plane wave $\propto \exp[iK(x\cos\theta + z\sin\theta)]$, of wavenumber magnitude K, in the hyperbolic equation, governing the perturbation pressure p:

$$p_{xx} + p_{yy} - (4\Omega^2/\sigma^2 - 1)p_{zz} = 0, \tag{1.1}$$

where subscripts denote partial derivatives, and x, y and z refer to Cartesian coordinates, rotating around the vertical z. Poincaré (1885) derived (1.1) to describe the (inviscid) internal oscillations of a homogeneous fluid in a rotating ellipsoid. This equation needs to be solved subject to the requirement that the perpendicular velocity component (related to pressure derivatives) vanishes at the boundary. For an incoming plane wave of wavenumber $\boldsymbol{k}_i$, this requires the wavenumber $\boldsymbol{k}_r$ of the reflected wave to satisfy

$$\boldsymbol{n}\times\boldsymbol{k}_r = \boldsymbol{n}\times\boldsymbol{k}_i, \tag{1.2}$$

with $\boldsymbol{n}$ denoting the boundary's outward unit normal vector, making an angle α with the horizontal (Phillips 1963). Since the absolute value of the wave direction θ is fixed upon reflection, (1.2) can be rewritten as

$$K_i\sin(\alpha+\theta) = K_r\sin(\alpha-\theta), \tag{1.3}$$

which shows that, for arbitrary θ, the wave number magnitude is unchanged only when $\alpha = 0, \pi/2 \bmod \pi$; i.e. when the reflecting wall is perpendicular or parallel to the rotation axis, like the walls of an axial cylinder having endwalls perpendicular to the rotation axis. Such walls are thus said to possess a local reflectional symmetry. The full sphere and ellipsoid are anomalous in the sense that, though not directly obeying this reflectional symmetry, the focusing that occurs upon reflection is apparently exactly balanced by defocusing. The same happens in the infinitely long cylinder, whose axis is perpendicular to the rotation axis, which can be rigorously transformed to a channel of rectangular cross-sectional shape, obeying the local reflectional symmetry (Barcillon 1968). However, besides the ellipsoid and (vertically or horizontally oriented) cylinder, very few geometries exist for which closed-form, regular solutions of 'Poincaré's problem' are known (Greenspan 1968; Barcilon 1968). Its solution hinges on finding a suitable coordinate system that allows separation of variables, which requires the presence of some symmetry in the container shape. Even in a spherical shell, relevant to geophysical studies, local reflectional symmetry is sufficiently broken to prohibit closed-form solutions, and, consequently, leads to the development of singularities (Bretherton 1964; Stewartson 1971; Rieutord, Georgeot & Valdettaro 2001), so-called

wave attractors (Maas & Lam 1995). However, despite criticism (Bjerknes *et al.* 1933; Stewartson & Rickard 1969; Solberg 1936; Huthnance 1978; Hendershott 1981; Chapman 1982; Colin de Verdière & Schopp 1994), most commonly used approximative descriptions of waves in (thin) rotating shells, such as the quasi-geostrophic and Laplace tidal equations and their local approximations, the f- and β-plane equations (Miles 1974; Gill 1982), eliminate the ability to develop singularities. Here we present the results of a laboratory experiment in which the local reflectional symmetry is broken by adopting a rectangular tank with one sloping sidewall. It shows the physical relevance of inertial wave attractors and their geophysically important mean field effects. Clearly, such a case with broken symmetry is much more common than the delicate cases for which closed-form solutions can be found.

To appreciate what happens in a case with broken symmetry, consider an infinitely long, rotating channel supplied with a rigid lid. Assuming the solution to be independent of the along-channel coordinate, y say, equation (1.1) reduces to the wave equation in terms of spatial coordinates,

$$p_{xx} - (4\Omega^2/\sigma^2 - 1)p_{zz} = 0. \tag{1.4}$$

This determines the pressure as the sum of two functions that are constant on the mathematical characteristics, $x \pm z \tan\theta = \text{constant}$ (Maas *et al.* 1997). These lines are identical to the ray paths, along which energy propagates. In channels whose walls break the local reflectional symmetry there will be convergence of the rays (Phillips 1963). Sloping sides therefore act as a lens, and focus two-dimensional inertial waves upon an attractor, which is either a point (the apex) or a line (see the example in Figure 1*b*), depending on whether the characteristic slope is larger or smaller than that of the sloping wall. Focusing towards the apex was oberved for inertial waves in a truncated cone by Beardsley (1970) and for internal gravity waves in a wedge by Cacchione & Wunsch (1974). A line-shaped wave attractor was first observed for internal gravity waves (Maas *et al.* 1997), in a tank of similar cross-sectional shape to the one studied here. Only when some symmetry is present in the container (and focusing is absent, or balanced by defocusing) may one find regular eigenmodes. In terms of ray paths, such standing modes occur when each ray is periodic (Maas & Lam 1995), allowing separation of variables. Feeding energy into them will lead to secular growth and breaking (as Benielli & Sommeria (1996) observed in the case of internal gravity waves), when and where angular momentum decreases with increasing radius and centrifugal instability sets in (Rayleigh 1916). This reveals the resonant collapse as resulting from the symmetry of the tank employed, which should be absent in containers whose shape breaks the local reflectional symmetry.

An explicit two-dimensional solution (Maas & Lam 1995) is useful for three-dimensional containers of finite extent, when currents are parallel to the vertical sidewalls, such as rectilinear, internal-wave currents (Maas *et al.* 1997). But two-dimensional inertial waves have circular (anti-cyclonic) currents (Greenspan 1968), which have a component perpendicular to the plane endwalls. This requires one to address the much tougher, fully three-dimensional equation (1.1), and it is not *a priori* clear whether focusing will still occur. The following experiment, in a tank that is much longer in along-slope y- than cross-slope x-direction, however shows that, due to the presence of a sloping wall, inertial wave attractors still exist. This choice of geometry produces weak y-variations, $\partial_y \approx 0$, apparently rendering two-dimensional predictions in the (x, z)-plane, as in figure 1(b), useful.

2. Laboratory observation of inertial wave focusing

An experiment was carried out in the 13 m diameter, rotating platform in Coriolis-lab, Grenoble. A tank of width, length and height $54 \times 120 \times 40\,\mathrm{cm}^3$ (in the x-, y- and z-directions respectively), having a rigid lid and a sidewall sloping down to the middle, was positioned eccentrically with its long side parallel to the rim of the platform (centred 5.5 m from the axis, see figure 1*a*). The tank is filled with a well-mixed salt solution, so as to obtain a homogeneous fluid whose density matches that of the (spherical) polysterene particles, used for visualization purposes. The platform is first put into steady rotation (angular frequency, $\Omega_0 = 2\pi/T_0$, $T_0 = 46.17\,\mathrm{s}$), to which the fluid adjusts on a timescale $T_E \approx 30\,\mathrm{min}$, which provides a monotonically increasing, radial (and, within the tank, nearly planar) angular momentum distribution. Here the spin-up timescale $T_E = \Omega_0^{-1} E^{1/2}$, where Ekman number $E \equiv \nu/2\Omega_0 H^2 \approx 2 \times 10^{-5}$, for kinematic viscosity $\nu = 10^{-6}\,\mathrm{m^2\,s^{-1}}$ and depth $H = 0.4\,\mathrm{m}$ (Greenspan & Howard 1963). Perturbations are introduced by weakly modulating the angular frequency, $\Omega = \Omega_0(1 + \epsilon \sin \sigma t), \epsilon = 0.1$, with a frequency $\sigma = 2\pi/T_1$, $T_1 = 32.4\,\mathrm{s}$. This choice aims at establishing the (nearly) square-shaped attractor of figure 1(*b*), see Maas *et al.* (1997). Particle image velocimetry (Fincham & Spedding 1997) is used to obtain top (figure 2*a*) and plan (figure 2*b*) views of the velocity field on a 61×45 grid. With this method, motions are visualized by illuminating particles within a laser sheet, which are followed by a digital video camera. The laser is intentionally kept out of focus (1 cm 'sheet width'), enabling tracking of particles despite some cross-sheet displacement. Velocity fields within the plane of the laser sheet are obtained by comparing patterns in two subsequent images (taken 0.25 s apart). Additional information on the flow is obtained by following the spreading of dye.

When the tank accelerates and decelerates, the Euler body force $\boldsymbol{x} \times \mathrm{d}\boldsymbol{\Omega}/\mathrm{d}t$ produces an alternating, vorticity-conserving, horizontal circulation cell (van Heijst, Maas & Williams 1994). Figure 2(*a*) displays this flow in the right half of the tank. This inviscid flow is subject to friction near the walls, where adjacent fluid quickly adjusts to the velocity of the container. In a rotating fluid, such (Ekman) boundary layers (Greenspan 1968) are of limited extent ($\delta_E = E^{1/2} H = O(0.2)\,\mathrm{cm}$), and are therefore badly resolved by measurements, but carry mass in the direction of the ambient, radial pressure gradient. Convergence and subsequent divergence of these boundary mass fluxes, together with the vertical flow directly induced by horizontal motion perpendicular to the slope, finally leads to the forcing of the inertial waves via periodic mass exchange with the (inviscid) interior. Surprisingly, even though the exact spatial location where this happens is not precisely known, and is probably spread out, the convergent nature of inertial wave characteristics predicts the fate of the waves rather well. For, after a second adjustment period (of some 20 min), a quasi-stationary pattern appears (figure 2*b*), which, in the in-plane component of the kinetic energy, bears the nearly square-shaped feature of an inertial wave attractor (figure 2*c*), predicted for this ratio of modulation and angular frequencies. Notice that the in-plane component of kinetic energy is not by itself conserved. Hence, each of the branches of the attractor vary in intensity over a cycle, but overall its square-shaped pattern remains visible.

Vivid support for the existence of the inertial wave attractor comes from the clockwise propagation of energy along the four sides of the attractor as inferred from the phase propagation in figure 3 and consistent with the focusing direction of characteristics (figure 1*b*). 'Phase' of the wave is identified with some observable, periodically varying property of the motion, here taken as the angle of the velocity vector with the horizontal, $\tan^{-1}(w/u)$. Near the bottom (figure 3*a*), at $z = 5\,\mathrm{cm}$,

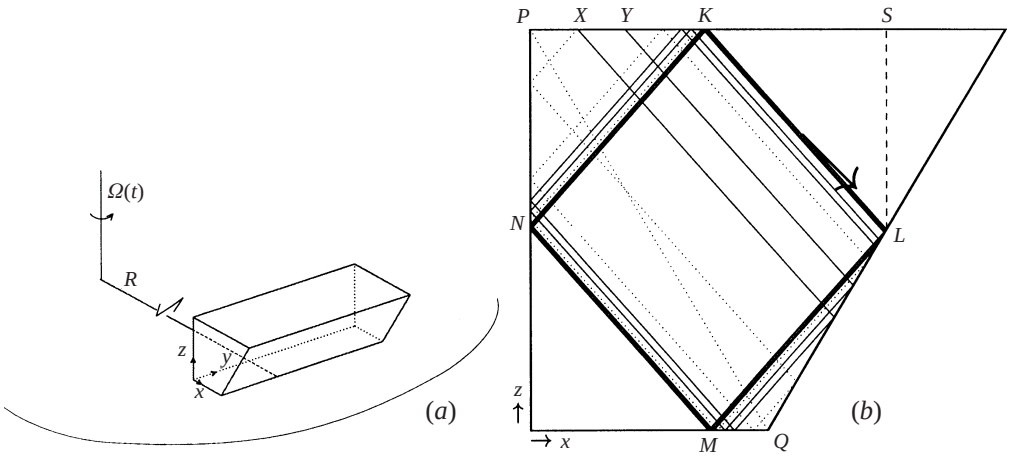

FIGURE 1. (*a*) Sketch of the experimental configuration in which a rigid-lid tank with a sloping wall, and filled with homogeneous water, is excentrically situated on a platform whose rotation speed $\Omega(t)$ is weakly modulated sinusoidally, $\Omega(t) = \Omega_0(1 + \epsilon \sin \sigma t)$, $\epsilon \ll 1$. Distance of the central axis of the tank to the platform's rotation axis R equals 5.5 m. The local x, y, z coordinate frame of reference, used further on, is indicated. (*b*) Sketch of vertical cross-section of container in (*a*). The tank is filled with homogeneous fluid, that is 'stratified' in angular momentum (in this two-dimensional-plane, increasing with increasing x). Some characteristics (lines along which energy propagates) of strictly two-dimensional inertial waves are followed, to the right as solid lines (from X and Y), showing their convergence upon reflection from the slope, and to the left as dotted lines (from X). For the particular ratio of perturbation and angular frequencies shown here, these characteristics all converge on the square-shaped attractor $KLMN$ (along which energy propagates in the clockwise direction, denoted by the arrow). A second modulation frequency employed in the experiments and referred to in the text, corresponds (nearly) to a degenerate line attractor, the dotted line PQ.

horizontal phase propagation (denoted by an arrow) is towards the sloping wall (coloured green), while near the top (figure 3*b*), at $z = 35$ cm, it propagates away from the sloping wall. As horizontal components of energy and phase propagate in opposite directions, this implies that near the bottom energy propagates away from, and near the top towards, the sloping wall. Vertical phase and energy propagation are aligned and upward next to the vertical sidewall (figure 3*c*), and downward over the sloping region (figure 3*d*) (apart from some unexplained upward motion in the higher regions). The resulting clockwise energy propagation in the (x, z)-plane is consistent with that predicted by the converging characteristics (figure 1*b*). A movie of contour plots of the phase clearly reveals a phase pattern with a saddle in the centre of the square-shaped attractor, and with phase flow towards the sloping wall (and opposite corner). These results suggest that a classical experiment in a concentric, truncated cone (Beardsley 1970; Henderson & Aldridge 1992) should be reinterpreted as showing wave attractors, rather than eigenmodes (Maas *et al.* 1997).

2.1. *Generation of mean flow*

Indirect evidence for the existence of an inertial wave attractor comes from considering the consequences of the intensification of inertial wave energy. Ensuing centrifugal instabilities will mix angular momentum, particularly at the radius where the attractor reflects from the slope, where the focusing takes place (at position L in figure 1*b*). To appreciate what this mixing implies, consider the angular momentum rv of a mixture of two equal quantities of solidly rotating fluid (azimuthal velocity $v = r\Omega$), coming from radii r_1 and $r_2 > r_1$, found at $\bar{r} = (r_1 + r_2)/2$: $\bar{r}\bar{v} \equiv (r_1 v_1 + r_2 v_2)/2$.

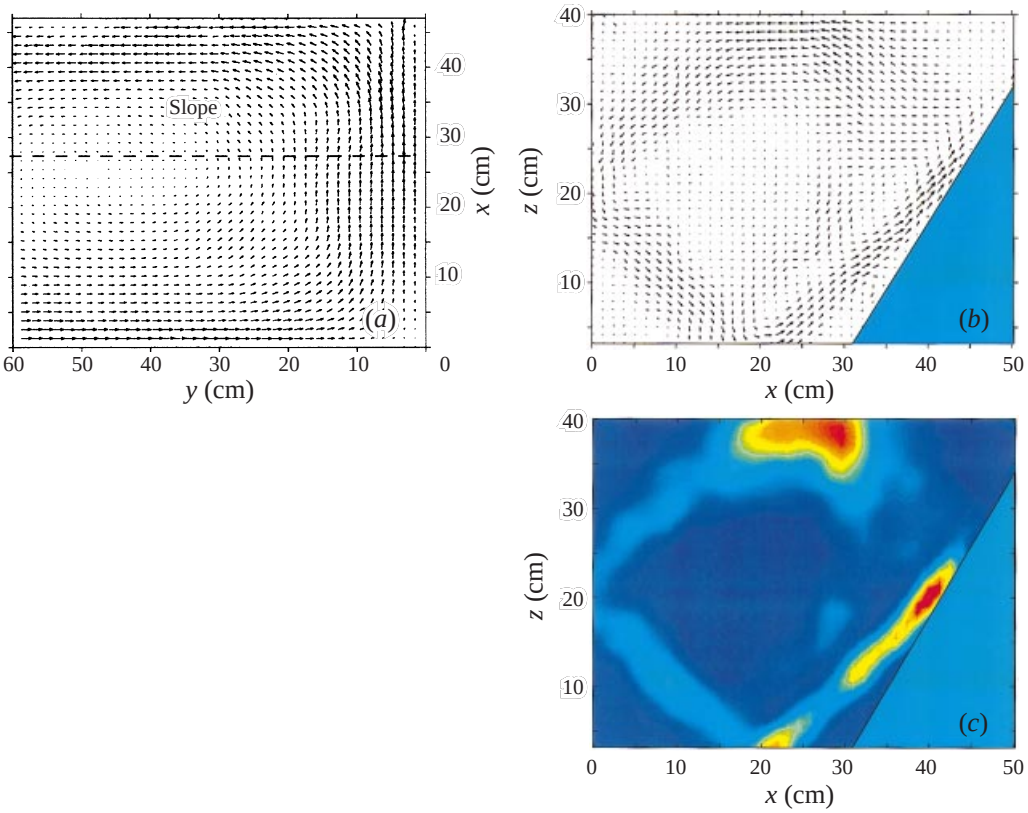

FIGURE 2. (*a*) Velocity observations (u, v) in a horizontal x, y-section of the right half of the tank, at $z = 30\,\mathrm{cm}$ above the bottom. The sloping wall is in the upper half of this figure, above the dashed line ($x > 27\,\mathrm{cm}$). Vertical, solid walls are at $x, y = 0$. The maximum velocity in this figure is $0.48\,\mathrm{cm\,s^{-1}}$. (*b*) Velocity observations (u, w) in a vertical x, z-section, at $y = 25\,\mathrm{cm}$ from the front wall, at a particular instant of the quasi-periodic state, showing focused inertial waves of modulation period. The maximum velocity in this plane is $0.32\,\mathrm{cm\,s^{-1}}$. Notice that the bottom 3 cm and upper right hand corner contain no observations. (*c*) False-colour (and smoothed) pattern of in-plane component of kinetic energy, $u^2 + w^2$, corresponding to (*b*).

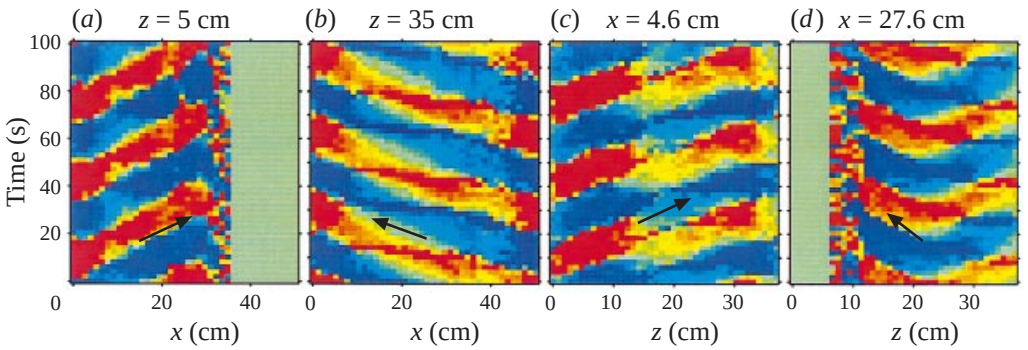

FIGURE 3. Phase, $\tan^{-1}(w/u)$, of the (u, w) velocity vector in the vertical plane at $y = 25\,\mathrm{cm}$, shown, along the ordinate, as a function of time and, along the abscissa, as a function of horizontal distance at fixed height, (*a*) $z = 5\,\mathrm{cm}$, and (*b*) $z = 35\,\mathrm{cm}$, or as a function of height at fixed distance from the vertical wall, (*c*) $x = 4.6\,\mathrm{cm}$ and (*d*) $x = 27.6\,\mathrm{cm}$. Arrows indicate phase progression.

The ratio of this quantity to the amount present at that location before mixing is $A = \bar{r}\bar{v}/(\bar{r}^2\Omega) = 2(r_1^2+r_2^2)/(r_1+r_2)^2$, thus giving the local velocity, after mixing, relative to that of a solid body, as $A = \bar{v}/(\bar{r}\Omega) = 2/[1 + 2/(r_1/r_2 + r_2/r_1)]$. As $1 < A < 2$, mixing of angular momentum thus means the generation of a cyclonic mean flow (Thompson 1979). Notice that in this example mixing is presented as a single event. In reality, this is a continuous process, leading to acceleration of a mean flow (Thompson 1970), whose final, observable magnitude is determined by (here unresolved) damping mechanisms. In analogy to the horizontal spreading of a mixture of density-stratified fluid along a gravity-potential surface, this accelerated water will now spread out axially, along a surface of the centrifugal potential (Thompson 1979). Therefore, we expect the mean flow generated at L to be present over the whole depth (along line LS in figure 1*b*). (This might also have caused the observed mean flow in a similar experiment in a paraboloid (Bretherton, Carrier & Longuet-Higgins 1969).)

To verify this, dye was injected at the quasi-steady state, through holes in the upper glass surface, and its evolution was followed by camera from above (see the two pictures, taken 6 modulation periods apart, in figure 4*a*, *b*). Apart from a horizontal oscillation of the dye, following the inviscid response of the fluid (see figure 2*a*), a remarkable net cyclonic, horizontal drift is observed over the central part of the sloping wall (upper half of figure 4*a*, *b*, at $x \approx 40$ cm), which is confirmed by direct observation of the time-averaged velocity (figure 4*e*), and which is clearly detached from the intersection of this plane with the slope (at $x = 46$ cm). A return flow due to continuity (at $x \approx 2$ cm), visible at the bottom of this picture, does stick to the (vertical) wall. The maximum velocity in this plane is $0.13\,\mathrm{cm\,s^{-1}}$, which agrees well with the 26 cm displacement of the dye tip, occurring at the mid-slope position over 194.4 s period, inferred from combining panels (*a*) and (*b*).

In contrast, such a drift is absent when the modulation period is changed to $T_1 = 37.7$ s, when the attractor nearly degenerates into line PQ of figure 1(*b*). Ray tracing (not shown) reveals that the line is still attracting, but viscous damping in the interior of the fluid apparently inhibits the concentration of energy upon the attractor (and subsequent mixing and mean-flow generation), and dye simply spreads diffusively (figure 4*c*, *d*). This can be understood since the fluid motion along two opposite sides of a rectangular-shaped attractor (such as KL and MN in figure 1(*b*) for a square-shaped attractor) may be parallel to these sides, but is out of phase, leading to strong shearing when these sides approach one another (upon change of the frequency of the wave, such that its attractor deforms into a line). For this case no particle image velocimetry is available.

3. Geophysical implications

3.1. *Forcing of equatorial currents*

The relevance of inertial wave attractors and their attendant mean flows for 'geophysical containers', such as oceans and lakes, which are not only clearly asymmetrically located with respect to the rotation axis, but also have sloping boundaries, is obvious. Even geometries which at first sight seem symmetric, such as the rotating spherical shell, relevant as descriptions of planetary atmospheres and cores, reveal, at a second glance, that they break the local reflectional symmetry of the centrifugal potential. However, a discussion of inertial waves proper (let alone their focusing) is rare. This is because in the 'traditional approximation' (Eckart 1960; Phillips 1966, the angular velocity component that is tangent to the Earth is neglected, while the hydrostatic

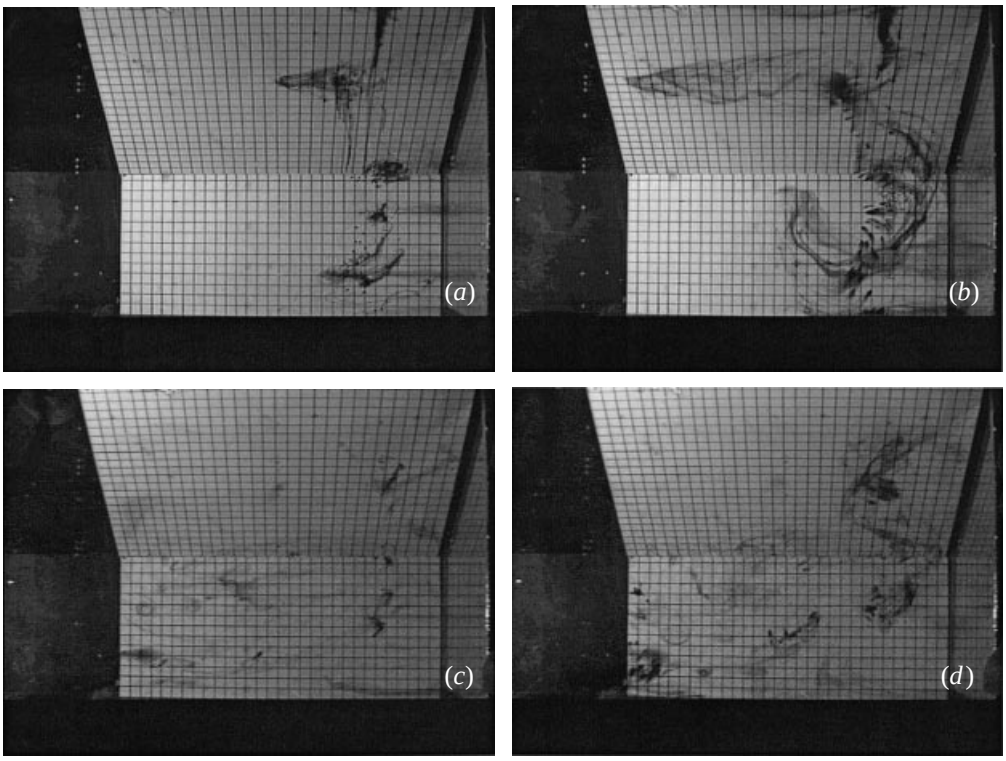

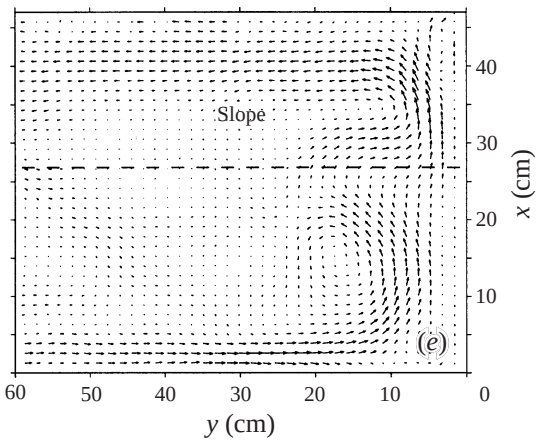

FIGURE 4. (*a*) Top view of the right half of the container, with the sloping wall visible in the upper half of the figure. The bottom and sloping wall have been supplemented with a 2 cm grid (distorted along the slope). Dye has been injected through a number of holes (of diameter $\approx$ 1 mm) in the glass top lid, at 14 cm from the vertical glass wall, at the right ($y = 0$). Modulation period is 32.4 s. Dye pictures, shown here, are taken at the moment that the dye reaches its most rightward position over the slope. (*b*) Picture taken 6 modulation periods after that in (*a*), showing the clear leftward spreading of dye over the central part of the slope in the upper half of the figure (revealing a cyclonic mean flow, i.e. in the same direction as the anti-clockwise background rotation). (*c*) As in (*a*), but with modulation period 37.7 s. Dye injections have additionally been made at some holes in the centre, and on the lower left of this figure. (*d*) As in (*c*), but taken 5 periods later. Dye seems to have spread diffusively. No signs of significant mean flow were observed in this case. (*e*) Top view of observed (time-averaged) mean flow at height $z = 30$ cm, when modulation period is as in (*a*) and (*b*). The foot of the slope (at $x = 27$ cm) is denoted by a dashed line.

approximation is also generally made. These approximations, on the f-plane reducing inertial waves to non-propagating oscillations, are formally justified (in off-equatorial regions) because of the presence of density stratification (Hylleraas 1939; Miles 1974), but must ultimately be motivated by the observed omni-presence of strong local inertial oscillations (of frequency $2\Omega \sin\phi$, at latitude ϕ), that seem to favour the perpendicular component of the angular velocity. The traditional approximation, however, fails in the equatorial zone, where gravity and centrifugal potential surfaces are parallel. The existence of approximate, trapped wave solutions of a rotating, homogeneous fluid in the equatorial zone (Stern 1963), described essentially by (1.4), led to the discovery that such a shell indeed carries periodic characteristic patterns (Bretherton 1964), which are attracting (Stewartson 1971; Hendershott 1981; Rieutord *et al.* 2001) and exist over continuous frequency bands (Israeli 1972). This suggests that inertial waves, generated around the equator by broad-band forcing, approach attractors, leading to centrifugal instabilities and, hence, mix angular momentum at their reflections from the ocean surface (where they get focused) and thus generate an eastward (cyclonic) zonal mean flow, which spreads out axially, along its potential surface. Conceptually, this can clearly contribute to observed equatorial countercurrents, as well as undercurrents (interpreted as belonging to the same axial surface, see Figure 5*a*). As fluid in a spherical shell in solid body rotation has the highest possible angular momentum at the surface of the equator, mixing can only reduce angular momentum there, necessarily leading to westward surface flow. This mixing mechanism might thus contribute to the observed equatorial current pattern, paralleling that produced by the wind (Gill 1982) and might be relevant to the enigmatic and persistent deep zonal current patterns, observed in the near-equatorial regions (Talley & Johnson 1994; Firing, Wijffels & Hacker 1998; Richardson & Fratantoni 1999; Muench & Kunze 1999). It may also be relevant for the quasi-biennial oscillation of the equatorial, lower stratosphere that, according to Sato & Dunkerton (1997), might be driven by gravito-inertial waves (rather than Kelvin and mixed Rossby–gravity waves). Thus, if geometric focusing of inertial waves and subsequent mixing is of relevance to zonal current patterns as observed in the ocean, stratosphere and planetary atmospheres, all that is perhaps needed to produce them is a liquid, rotating, spherical shell, supplemented with low-frequency ($\sigma < 2\Omega$) noise.

In Poincaré's non-stratified model, gravity dominates centrifugal effects in determining the oblate (disk-like) spheroidal shape of the inner and outer boundaries of the 'fluid container' (here approximated by spheres). But, perturbations of this contained, homogeneous fluid no longer 'feel' gravity, and are exclusively restored by centrifugal (Coriolis) forces, so that rays are straight lines, as in figure 5(*a*). Correspondence with reality may be claimed in the near-equatorial zone of the ocean only (when applied to the gravito-inertial frequency band), where centrifugal and buoyancy forces co-align. The real ocean, however, is also stratified (radially, in a first approximation), and buoyancy (gravity) forces again dominate. Investigations of such a rotating, radially stratified liquid shell show that a hyperbolic, gravito-inertial wave regime, and therefore also wave attractors, continue to exist, but with characteristics that get bent, and that reflect from a turning surface that borders the spatial domain over which (1.1) applies (Friedlander & Siegmann 1982; Dintrans, Rieutord & Valdettaro 1999). In a non-rotating, stratified spherical shell, any mixture would spread tangentially, along a spherical potential surface. The previously noted axial spreading of water whose angular momentum was mixed in the homogeneous, rotating case, however, makes it clear that in the combined case of a rotating, radially stratified liquid shell, even when buoyancy forces dominate over Coriolis forces, spreading of a mixture will no longer

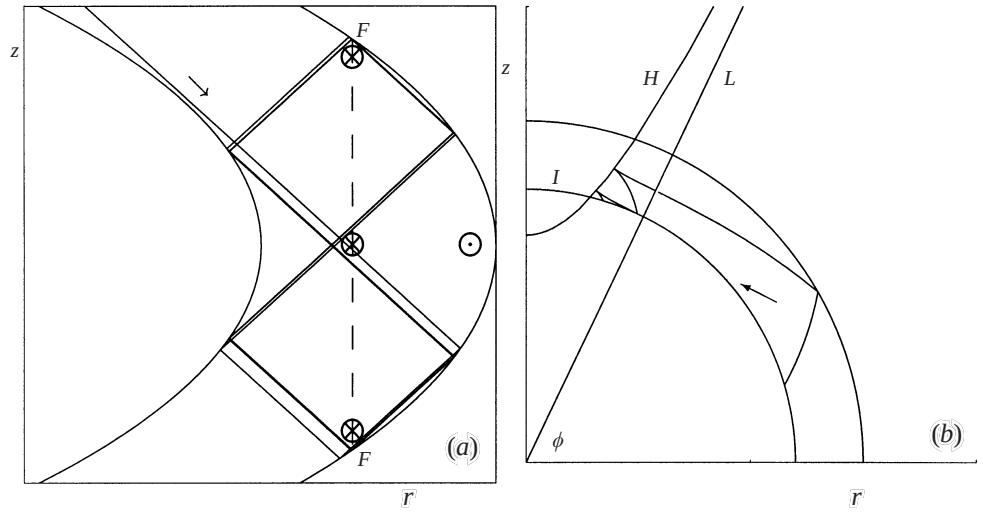

FIGURE 5. Sketch of characteristics (solid lines) in a vertical cross-section of a rotating spherical shell filled with (*a*) homogeneous fluid, and (*b*) fluid that is density-stratified radially. Rotation axis z is along the ordinate; cylindrical distance r along the abscissa. (*a*) Demonstrates equatorial trapping (Bretherton 1964) and focusing of characteristics (and waves), leading to mixing of angular momentum. This accelerated water will subsequently spread axially (dashed line) from focusing locations F, leading to a band of eastward (cyclonic) flow, $\otimes$, like the oceanic, near-surface north and south equatorial countercurrents, and like the subsurface equatorial undercurrent. At the surface of the equatorial plane, angular momentum mixing decelerates fluid, predicting an (anti-cyclonic) westward flow, $\odot$, like the oceanic surface equatorial current. Notice that for visual clarity this figure has been compressed in the axial direction by a factor 4. (*b*) Demonstrates trapping (energy following the arrow) of (bent) characteristics (and waves) in the wedge formed by hyperbolic turning surface H and inner sphere I (in the ocean, extending a few tens of kilometres north of the inertial latitude ϕ, which is line L to which H tends asymptotically), see Dintrans *et al.* (1999).

be strictly along spherical potential surfaces, but diapyncal, along prolate (rugby-ball shaped) spheroids. In the cross-sectional plane, shown in figure 5(*a*), this will be along ellipses, elongated in the axial z-direction, intersecting the outer spherical shell, thus retaining the same topological features: westward flow at the surface on the equator, and eastward flow of mixed (zonally accelerated) water in the north and south equatorial regions, which may again spread from the surface downwards and equatorwards, albeit much less deep than in a homogeneous case, in line with the observed depth of the equatorial undercurrent being much less than predicted for the homogeneous case. Given the smallness of the frequency windows over which (physically realizable) large-scale attractors appear (Stewartson 1971; Tilgner 1999; Rieutord *et al.* 2001), and considering the general sensitiveness of the shape of the attractor to the details of the description of the medium (geometry, stratification and current shear, see Maas & Lam 1995), a fair quantitative comparison deserves these factors to be incorporated more carefully than can be done here. Suffice it to state that very strong mixing close to the surface has indeed been observed in the north equatorial countercurrent (Perkins & Van Leer 1977), in line with the above expectation. Further work is needed to find out which frequency window might be responsible for the large-scale attractors, and to see if there is any evidence for spatial enhancement of that particular frequency band within the equatorial countercurrent regions. The most fascinating question will be to see whether the tidal frequencies may actually be situated in one of these 'attracting windows', which might boost their

importance, in a similar way to that recently proposed with respect to the general ocean circulation (Munk & Wunsch 1998).

3.2. *Inertial oscillations*

The remarkable fact that basic properties like stable stratification, rotation, and irregular shape, of some 'fluid envelopes', like the ocean, lead to the prevalence of wave attractors in a hyperbolic wave regime with its ensuing mixing, and mean flow generation, not only urges a search for oceanic wave attractors, but also forces us to recognize the limitations of many present-day, large-scale ocean models, that simply do not allow for wave attractors.

A case in point is inertial oscillations, which are commonly observed in the ocean (Webster 1968; Fu 1981), being a spectral peak of velocity records at or slightly above frequency $\sigma = 2\Omega \sin\phi$, where ϕ is the latitude where the measurements are taken. Significantly, these oscillations show a higher coherence between horizontal or diagonally separated current meters, than between vertically separated ones (Anderson, Huyer & Smith 1983), have a relatively small horizontal lengthscale ($< 10\,\mathrm{km}$) (Kunze & Sanford 1984; d'Asaro 1984), and often occur at great depths ($> 300\,\mathrm{m}$), as for instance, in the tideless Black Sea (Golubev 1995), raising the need for an amplification mechanism of observed, large, persistent deep inertial waves (Kundu 1993).

Previous theories have either interpreted inertial oscillations as being locally excited at the surface at latitude ϕ, say, which then act as a source region, from which waves of that frequency σ can propagate equatorwards (for which the local inertial frequency is less), as gravito-inertial waves (Garrett 1999), or as turning point enhancement of poleward propagating and subsequently reflecting gravito-inertial waves of given frequency σ, arising from the equatorial belt between latitudes $\pm\phi = \pm\sin^{-1}\sigma/2\Omega$ (Munk & Phillips 1968; Stewartson & Walton 1976; Fu 1981). The present model, recognizing the curvature in the turning surface, suggests that these poleward gravito-inertial waves may actually be trapped in the wedge formed by the turning surface (very close to the inertial latitude (Friedlander & Siegmann 1982)) and bottom (Dintrans *et al.* 1999), see figure 5(*b*), thus explaining the ubiquitous build-up of energy at, what is reversely called, the inertial frequency, $f = 2\Omega \sin\phi$, which then acts as a sink (point attractor). The final approach to the bottom agrees with observed, predominantly downward inertial wave energy propagation, close to the inertial latitude (Leaman & Sanford 1975; d'Asaro & Perkins 1984). Significantly, inertial oscillations have been observed in the stably stratified, lower stratosphere (Thompson 1978; Ushimara & Tanaka 1990; Hu & Holzworth 1997), while they are inconspicuous in the much weaker stratified troposphere (Holton 1979), in agreement with the fact that the homogeneous spherical shell lacks such a trap.

3.3. *Universality of gravito-inertial wave spectra*

Breaking the local reflectional symmetry of characteristics in the axial plane leads to wave attractors, as shown rigorously in a two-dimensional setting, and as made plausible by the above experiment in a three-dimensional container. Interestingly, the Poincaré problem (1.1) includes a complementary behaviour, with divergent (chaotic) ray paths, when the symmetry of the problem is broken in the horizontal plane. This is possibly of relevance in understanding the canonical nature of oceanic, gravito-inertial wave spectra (Garrett & Munk 1975; Munk 1980).

This behaviour is obtained when the container surfaces respect the reflectional symmetry, and are strictly parallel or perpendicular to the rotation axis (z). Reflection

at these surfaces now leaves the vertical distance between rays unaffected, allowing for vertically standing waves, $p = P(x, y)\cos mz$, obeying impermeability of the horizontal (rigid lid) surface and bottom for appropriately chosen m. The horizontal structure of the wave field, $P(x, y)$, is then described by an elliptic (Helmholtz) equation

$$P_{xx} + P_{yy} + m^2(4\Omega^2/\sigma^2 - 1)P = 0. \tag{3.1}$$

In quantum mechanics, this is studied as a special case of Schrödinger's equation, where P represents the wave function of an electron in an infinitely deep well (at zero potential). Depending on the shape of the basin (well) in the horizontal plane, this equation supports either chaotic wave functions, or regular eigenmodes (Berry 1987). The Helmholtz equation reduces to a tractable dynamical system (a two-dimensional map), when one considers high-energy, short waves (large m). These waves again propagate along straight lines–ray paths, but now reflect from sidewalls specularly (Heller 1996). In this limit, the dynamics is described by the fate of the rays, and one aims at identifying the density of ray paths with the probability density of the wave function, $|P|^2$. For a number of well shapes, the ray paths are chaotic, hence this field is referred to as quantumchaos (Gutzwiller 1990). Chaotic wave functions correspond to ergodic orbits (on which only energy is conserved), while regular eigenmodes correspond to closed orbits, which are rendered integrable by the presence of a second conserved quantity (angular momentum) due to some symmetry of the bounding shape (as for a circle), see examples in Berry (1981). Ergodic orbits, associated with the chaotic spread of short waves, may perhaps also offer an explanation for the observed universality in gravito-inertial wave spectra in the ocean (Garrett & Munk 1975; Munk 1980). In this case, one has to regard the filling of the ocean's spectrum to be due to rapid, nonlinear processes, close to the source (surface, bottom, or shelf edge) (Wunsch 1976), while the subsequent spreading of the resulting small-amplitude linear waves might be along chaotic orbits, leaving, by scattering from the (irregular) ocean boundary, an overall universal impression.

It is interesting to note that, even in this chaotic regime, periodic orbits, despite being repelling, again seem to dominate the distribution of ray paths. This is because waves tend to linger in their neighbourhood, and thus build up a significant amount of energy there, producing 'scars' (Gutzwiller 1990; Heller 1996), that are surprisingly reminiscent of their attracting counterparts in the hyperbolic wave regime.

4. Summary

In this paper we have looked at inertial waves in a homogeneous, rotating, fully contained fluid. Previous laboratory experiments, (two-dimensional) theory, and numerical work suggest that perturbations of the uniformly rotating state will give rise to inertial wave focusing when some of the walls are not entirely parallel or perpendicular to the rotation axis, so that the local reflectional symmetry of the container is broken. The occurrence of an inertial wave attractor, as the result of repeated focusing, has here been verified experimentally, by using a container with one sloping sidewall. Though this may at first sight seem a peculiarity of this particular choice of geometry, it should be realized that almost all natural containers will break the local reflectional symmetry, and the occurrence of wave attractors should thus be regarded as a generic phenomenon. Only by a very careful choice of geometry can focusing be avoided. Ironically, this is quite often the case in the laboratory, where upright cylindrical or rectangular domains are generally favoured. Indeed, in Faller's terminology (Faller 1981), the present experiment is classified as an 'abstract experiment', intended to isolate a particular conceptual process believed to be significant in nature.

Not only is the focusing phenomenon often eliminated in the lab (by an unfortunate choice of geometry), but, more seriously, also in most commonly used theoretical descriptions of wave motion in geophysics (due to a combination of the 'traditional' and hydrostatic approximation). These 'symmetrizing' approximations are, however, avoided in Poincaré's equation (1.1), which is the central (linear) model used here.

The present laboratory experiment shows that focusing is accompanied by the generation of a cyclonic mean flow, along the axial cylinder that intersects the sloping bottom at the position where the focusing takes place. This is argued to be the result of centrifugal instabilities, due to the mixing of angular momentum, occurring upon intensification of the current shear. In the geophysical context, the spherical shape of the boundaries gives rise to inertial wave attractors, which may have relevance to the driving of mean currents along the axial cylinder that intersects the surface focusing locations (labelled F, in figure 5*a*). At these surface locations, and at the sub-surface equator, this will be perceived as eastward countercurrents. The presence of stratification will modify the spreading of the mixture (deforming the axial cylinder into a prolate ellipsoid), but not the topology of the mean currents.

When (strong) stratification is added, the physically penetrable wave domain is spatially restricted (by the occurrence of a turning surface). But numerical work (Dintrans *et al.* 1999) suggests that wave attractors continue to exist. The ubiquitous inertial peak in ocean spectra may in fact reflect the presence of a particular, degenerate type of attractor, namely a point attractor (at the intersection of the bottom and turning surface), which acts as a trap for gravito-inertial waves from the equatorial belt that are steered polewards by reflections from the surface, bottom and turning surface.

Even when a container does respect the local reflectional symmetry, yet another type of symmetry breaking may occur, namely one which destroys the periodicity of rays in the horizontal plane. This may lead to the complementary situation of wave chaos, which may be relevant to the apparent universality of oceanic gravito-inertial wave spectra. In real geophysical containers both symmetries will often be broken, so that one may anticipate observations of both focusing and wave chaos. As these two phenomena arise in approximations of the Poincaré equation (1.1), further study of the full three-dimensional Poincaré problem seems warranted.

The author gratefully acknowledges the hospitality and support from D. Renouard, A. Fincham, J.-B. Flór, H. Didelle and R. Carcel, of Coriolis-Lab Grenoble, where experiments were performed under the auspices of the EC-TMR Large Scale Facility program. Help during the experiments and post-processing by F. Eijgenraam and N. Pörtzgen, and comments by J. T. F. Zimmerman, Th. Gerkema and H. van Haren are deeply appreciated. Thanks are also due to M. Rieutord and an unknown referee for perceptive comments on the first version of this paper. This is NIOZ contribution no 3518.

REFERENCES

Aldridge, K. D. & Lumb, L. I. 1987 Inertial waves identified in the earth's fluid outer core. *Nature* **235**, 421–423.

Anderson, I., Huyer, A. & Smith, R. L. 1983 Near-inertial motions off the Oregon coast. *J. Geophys. Res.* **88**, 5960–5972.

d'Asaro, E. A. 1984 Wind forced internal waves in the North Pacific and Sargasso Sea. *J. Phys. Oceanogr.* **14**, 781–794.

d'Asaro, E. A. & Perkins, H. 1984 A near-inertial internal wave spectrum for the Sargasso Sea in late summer. *J. Phys. Oceanogr.* **14**, 489–505.

Barcilon, V. 1968 Axi-symmetric inertial oscillations of a rotating ring of fluid. *Mathematika* **15**, 93–102.

Beardsley, R. C. 1970 An experimental study of inertial waves in a closed cone. *Stud. Appl. Maths* **49**, 187–196.

Benielli, D. & Sommeria, J. 1996 Excitation of internal waves and stratified turbulence by parametric instability. *Dyn. Atmos. Oceans* **23**, 335–343.

Berry, M. V. 1981 Regularity and chaos in classical mechanics, illustrated by three deformations of a circular 'billiard'. *Eur. J. Phys.* **2**, 91–102.

Berry, M. V. 1987 Quantum chaology. *Proc. R. Soc. Lond.* A **413**, 183–198.

Bjerknes, V., Bjerknes, J., Solberg, H. & Bergeron, T. 1933 *Physikalische Hydrodynamik*. Springer.

Bretherton, F. P. 1964 Low frequency oscillations trapped near the equator. *Tellus* **16**, 181–185.

Bretherton, F. P., Carrier, G. F. & Longuet-Higgins, M. S. 1969 Report on the I.U.T.A.M. symposium on rotating fluid systems. *J. Fluid Mech.* **26**, 393–410.

Cacchione, D. H. & Wunsch, C. 1974 Experimental study of internal waves over a slope. *J. Fluid Mech.* **66**, 223–239.

Chapman, D. C. 1982 On the failure of Laplace's tidal equations to model subinertial motions at a discontinuity in depth. *Dyn. Atmos. Oceans* **7**, 1–16.

Colin de Verdière, A. & Schopp, R. 1994 Flows in a rotating spherical shell: the equatorial case. *J. Fluid Mech.* **276**, 233–260.

Dintrans, B., Rieutord, M. & Valdettaro, L. 1999 Gravito-inertial waves in a rotating stratified sphere or spherical shell. *J. Fluid Mech.* **398**, 271–297.

Eckart, C. 1960 *Hydrodynamics of Oceans and Atmospheres*. Pergamon.

Faller 1981 The origin and development of laboratory models and analogues of the ocean circulation. In *Evolution of Physical Oceanography* (ed. B. A. Warren & C. Wunsch), pp. 462–479. MIT Press.

Fincham, A. & Spedding, G. R. 1997 Low cost, high resolution dpiv for measurement of turbulent fluid flow. *Exps. Fluids* **23**, 449–462.

Firing, E., Wijffels, S. & Hacker, P. 1998 Equatorial subthermocline currents across the pacific. *J. Geophys. Res.* **C10**, 21413–21423.

Friedlander, S. & Siegmann, W. L. 1982 Internal waves in a rotating stratified fluid in an arbitrary gravitational field. *Geophys. Astrophys. Fluid Dyn.* **19**, 267–291.

Fu, L. L. 1981 Observations and models of inertial waves in the deep ocean. *Rev. Geophys. Space Phys.* **19**, 141–170.

Fultz, D. 1959 A note on overstability and the elastoid-inertia oscillations of Kelvin, Solberg and Bjerknes. *J. Met.* **16**, 199–208.

Garrett, C. 1999 What is the "near-inertial" band and why is it different? In *Dynamics of Oceanic Internal Gravity Waves, Proc. 'Aha Huliko'a Hawaiian Winter Workshop* (ed. P. Müller & D. Henderson), pp. 215–222. SOEST.

Garrett, C. J. R. & Munk, W. H. 1975 Space-time scales of internal waves: a progress report. *J. Geophys. Res.* **80**, 291–297.

Gill, A. E. 1982 *Atmosphere-Ocean Dynamics*. Academic.

Golubev, Yu. N. 1995 About the origin of inertial oscillations in deep layers of the Black Sea. *Atmos. Ocean. Phys.* **30**, 490–496.

Görtler, H. 1943 Über eine Schwingungserscheinung in Flüssigkeiten mit stabiler Dichteschichtung. *Z. Angew. Math. Mech.* **23**, 65–71.

Görtler, H. 1944 Einige bemerkungen über Strömungen in rotierenden Flüssigkeiten. *Z. Angew. Math. Mech.* **24**, 210–214.

Gough, D. O. & McIntyre, M. E. 1998 Inevitability of a magnetic field in the Sun's radiative interior. *Nature* **394**, 755–757.

Greenspan, H. 1968 *The Theory of Rotating Fluids*. Cambridge University Press.

Greenspan, H. P. & Howard, L. N. 1963 On a time-dependent motion of a rotating fluid. *J. Fluid Mech.* **17**, 385–404.

Gutzwiller, M. C. 1990 *Chaos in Classical and Quantum Mechanics*. Springer.

Heijst, G. J. F. van, Maas, L. R. M. & Williams, C. W. M. 1994 The spin-up of fluid in a rectangular container with a sloping bottom. *J. Fluid Mech.* **265**, 125–159.

Heller, E. J. 1996 Quantum chaos for real. *Nature* **380**, 583–584.

Hendershott, M. C. 1981 Long waves and ocean tides. In *Evolution of Physical Oceanography* (ed. B. A. Warren & C. Wunsch), pp. 292–341. MIT Press.

Henderson, G. & Aldridge, K. D. 1992 A finite-element method for inertial waves in a frustum. *J. Fluid Mech.* **234**, 317–327.

Holton, J. R. 1979 *An Introduction to Dynamic Meteorology*, 2nd Edn. Academic.

Hu, H. & Holzworth, R. H. 1997 An inertial wave-driven stratospheric horizontal electric field: new evidence. *J. Geophys. Res.* D **102**, 19717–19727.

Huthnance, J. M. 1978 Inertial waves and an initial-value problem for a thin spherical rotating fluid shell. *J. Fluid Mech.* **86**, 273–288.

Hylleraas, E. A. 1939 Über die Schwingungen eines stabil geschichteten, durch Meridiane begrenzten Meeres. *Astrophysica Norvegica* **3**, 139–163.

Israeli, M. 1972 On trapped oscillations of rotating fluids in spherical shells. *Stud. Appl. Maths* **51**, 219–237.

Kelvin, L. 1880 Vibrations of a columnar vortex. *Phil. Mag.* **10**, 155–168.

Kundu, P. 1993 On internal waves generated by travelling wind. *J. Fluid Mech.* **254**, 529–559.

Kunze, E, & Sanford, T. B. 1984 Observations of near-inertial waves in a front. *J. Phys. Oceanogr.* **14**, 566–581.

Leaman, K. D. & Sanford, T. B. 1975 Vertical propagation of inertial waves: A vector spectral analysis of velocity profiles. *J. Geophys. Res.* **80**, 1975–1978.

LeBlond, P. H. & Mysak, L. A. 1978 *Waves in the Ocean.* Elsevier.

Maas, L. R. M., Benielli, D., Sommeria, J. & Lam, F.-P. A. 1997 Observation of an internal wave attractor in a confined stably-stratified fluid. *Nature* **388**, 557–561.

Maas, L. R. M. & Lam, F.-P. A. 1995 Geometric focusing of internal waves. *J. Fluid Mech.* **300**, 1–41.

Manasseh, R. 1992 Breakdown regimes of inertia waves in a precessing cylinder. *J. Fluid Mech.* **243**, 261–296.

Manasseh, R. 1996 Nonlinear behaviour of contained inertia waves. *J. Fluid Mech.* **315**, 151–173.

McEwan, A. D. 1970 Inertial oscillations in a rotating fluid cylinder. *J. Fluid Mech.* **40**, 603–640.

Miles, J. W. 1974 On Laplace's tidal equations. *J. Fluid Mech.* **66**, 241–260.

Muench, J. E. & Kunze, E. 1999 Internal wave interactions with equatorial deep jets. Part I: Momentum-flux divergences. *J. Phys. Oceanogr.* **29**, 1453–1467.

Munk, W. 1980 Internal wave spectra at the buoyant and inertial frequencies. *J. Phys. Oceanogr.* **10**, 1718–1728.

Munk, W. & Phillips, N. A. 1968 Coherence and band structure of inertial motion in the sea. *Rev. Geophys.* **4**, 447–472.

Munk, W. & Wunsch, C. 1998 Abyssal recipes II: energetics of tidal and wind mixing. *Deep- Sea Res.* I **45**, 1977–2010.

Olson, P. & Aurnou, J. 1999 A polar vortex in the Earth's core. *Nature* **402**, 170–173.

Oser, H. 1958 Experimentele Untersuchung über harmonische Schwingungen in rotierenden Flüssigkeiten. *Z. Angew. Math. Mech.* **38**, 386–391.

Perkins, H. & Van Leer, J. 1977 Simultaneous current-temperature profiles in the equatorial counter current. *J. Phys. Oceanogr.* **7**, 264–271.

Phillips, N. A. 1966 The equations of motion for a shallow rotating atmosphere and the "traditional approximation". *J. Atmos. Sci.* **23**, 626–628.

Phillips, O. M. 1963 Energy transfer in rotating fluids by reflection of inertial waves. *Phys. Fluids* **6**, 513–520.

Poincaré, H. 1885 Sur l'équilibre d'une masse fluide animée d'un mouvement de rotation. *Acta Math.* **VII**, 259–380.

Rayleigh, L. 1916 On the dynamics of revolving fluids. *Proc. R. Soc. Lond.* A **93**, 148–154.

Richardson, P. L. & Fratantoni, D. M. 1999 Float trajectories in the deep western boundary current and deep equatorial jets of the tropical atlantic. *Deep-Sea Res.* II **46**, 305.

Rieutord, M., Georgeot, B. & Valdettaro, L. 2001 Inertial waves in a rotating spherical shell: attractors and asymptotic spectrum. *J. Fluid Mech.*, **435**, 103–144.

Sato, K. & Dunkerton,T. J. 1997 Estimates of momentum flux associated with equatorial Kelvin and gravity waves. *J. Geophys. Res.* D. **102**, 26247–26261.

Solberg, H. 1936 Über die freien Schwingungen einer homogenen Flüssigkeitsschicht auf der rotierenden Erde. I. *Astrophysica Norvegica* **1**, 237–340.

Stern, M. E. 1963 Trapping of low frequency oscillations in an equatorial 'boundary layer'. *Tellus* **15**, 246–250.

Stewartson, K. 1971 On trapped oscillations of a rotating fluid in a thin spherical shell. *Tellus* **23**, 506–510.

Stewartson, K. & Rickard, J. A. 1969 Pathological oscillations of a rotating fluid. *J. Fluid Mech.* **5**, 577–592.

Stewartson, K. & Walton, I. C. 1976 On inertial oscillations in the oceans. *Tellus* **28**, 71–73.

Talley, L. D. & Johnson, G. C. 1994 Zonal subequatorial currents. *Science* **263**, 1125–1128.

Thompson, R. 1970 Diurnal tides and shear instabilities in a rotating cylinder. *J. Fluid Mech.* **40**, 737–751.

Thompson, R. O. R. Y. 1978 Observations of inertial waves in the stratosphere. *Q. J. R. Met. Soc.* **104**, 691–698.

Thompson, R. O. R. Y. 1979 A mechanism for angular momentum mixing. *Geophys. Astrophys. Fluid Dyn.* **12**, 221–234.

Tilgner, A. 1999 Driven inertial oscillations in spherical shells. *Phys. Rev.* E **59**, 1789–1794.

Ushimara, S. & Tanaka, H. 1990 Characteristics of internal inertial gravity waves and inertial waves in the lower stratosphere observed by the MU radar. *J. Met. Soc. Japan.* **68**, 1–18.

Veronis, G. 1970 The analogy between rotating and stratified fluids. *Ann. Rev. Fluid Mech.* **2**, 37–66.

Webster, F. 1968 Observations of inertial-period motions in the deep sea. *Rev. Geophys.* **6**, 473–490.

Wunsch, C. 1976 Geographical variability of the internal wave field: A search for sources and sinks. *J. Phys. Oceanogr.* **6**, 471–485.